Device

Report

Mechanically programming anisotropy in engineered muscle with actuating extracellular matrices

Graphical abstract

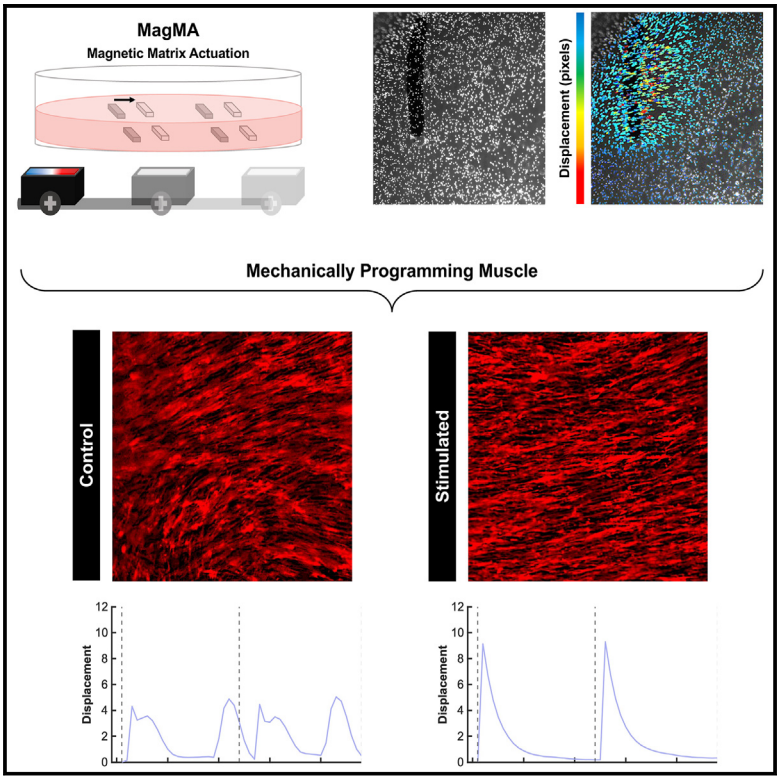

Highlights

- Magnetic microparticles are embedded in an extracellular-matrix-mimicking gel
- Controlled movement of a permanent magnet drives gel actuation
- Magnetic matrix actuation (MagMA) programs alignment of skeletal muscle fibers
- MagMA-aligned muscle tissues generate synchronous contractile twitch

Authors

Brandon Rios, Angel Bu, Tara Sheehan, ..., Karina Shah, Emma Lejeune, Ritu Raman

Correspondence

ritur@mit.edu

In brief

Living cells embedded in an extracellular matrix sense and respond to mechanical stimuli in their environment. We have developed a method for magnetic matrix actuation (MagMA) enabling dynamic, non-invasive mechanical stimulation of tissues. As a proof-of-concept demonstration, we show that MagMA programs the alignment of skeletal muscle fibers with downstream functional effects on the global synchrony of muscle contraction. Precisely controlling muscle morphology and force generation is of significant importance in applications ranging from regenerative medicine to robotics.

Explore
Early prototypes with exciting performance and new methodology

Rios et al., 2023, Device *1*, 100097
October 20, 2023 Published by Elsevier Inc.
https://doi.org/10.1016/j.device.2023.100097

CellPress

Device

CellPress
OPEN ACCESS

Report

Mechanically programming anisotropy in engineered muscle with actuating extracellular matrices

Brandon Rios,[1,3] Angel Bu,[1,3] Tara Sheehan,[1] Hiba Kobeissi,[2] Sonika Kohli,[1] Karina Shah,[1] Emma Lejeune,[2] and Ritu Raman[1,4,*]

[1]Department of Mechanical Engineering, Massachusetts Institute of Technology, Cambridge, MA, USA
[2]Department of Mechanical Engineering, Boston University, Boston, MA, USA
[3]These authors contributed equally
[4]Lead contact
*Correspondence: ritur@mit.edu
https://doi.org/10.1016/j.device.2023.100097

THE BIGGER PICTURE Cells within tissues communicate with each other, and with their surrounding matrix, thorough biochemical, electrical, and mechanical signals. While there are a range of techniques for mapping and controlling electrical and biochemical communication within multicellular systems, there is a significant need for tools that measure and modulate mechanical stimuli in a similar manner. A platform for dynamically patterning forces within tissues would enable mechanically programming morphology and function of various adaptive mechanobiological processes.

SUMMARY

The hierarchical design and adaptive functionalities of biological tissues are driven by dynamic biochemical, electrical, and mechanical signaling between cells and their extracellular matrices. While existing tools enable monitoring and controlling biochemical and electrical signaling in multicellular systems, there is a significant need for techniques that enable mapping and modulating intercellular mechanical signaling. We have developed a magnetically actuated extracellular matrix that serves as a mechanically active substrate for cells and can program morphological and functional anisotropy in tissues such as skeletal muscle. This method improves the ease and efficiency of programming muscle force directionality and synchronicity for applications ranging from medicine to robotics. Additionally, we present an open-source computational framework enabling quantitative analyses of muscle contractility. Our actuating matrices and accompanying tools are broadly applicable across cell types and hydrogel chemistries, and they can drive fundamental studies in mechanobiology as well as translational applications of engineered tissues in medicine and machines.

INTRODUCTION

Multicellularity is the key to the dynamic functionality of biological tissues. Cells embedded in an extracellular matrix communicate with each other, and with their surrounding scaffold, through a combination of chemical, electrical, and mechanical signaling.[1] While scientists have developed a range of tools for mapping and modulating electrical and chemical signaling within tissues, including microinvasive electrodes and nanofluidic probes,[2,3] there remains a significant need for robust tools that can actively tune intercellular mechanical signaling. Techniques for mechanical measurement such as traction force microscopy and stretchable biosensors can offer insight into the forces generated by living cells,[4,5] but they are designed for passive observation rather than for active modulation of mechanical signaling. Methods for actively imposing forces on multicellular systems have largely focused on actuated stretching and compression devices for whole-tissue stimulation,[6,7] which do not replicate the spatial modulation of forces observed in natural systems. A soft actuating substrate capable of controlling cell-cell mechanical interaction with high spatiotemporal precision could be used to probe the impact of external forces on intercellular communication and to measure downstream impact on morphology and function. Such a material would be an impactful enabling technology for engineering tissues from a range of cell types known to be impacted by mechanical signaling.[8–12]

Several recent studies have reported active hydrogels controlled by external stimuli such as light, heat, pH, magnetic,

and chemical inputs.[13–24] Optically and magnetically responsive hydrogels have, in particular, proven highly compelling as cell substrates as they are spatially controllable and non-contact, thereby limiting off-target effects on cells.[19,22,23,25,26] However, most prior studies on actuating hydrogels as cell substrates have focused on dynamic stiffness modulation or 3D shape transformation[22,23,27–29] rather than on the in-plane actuation that more closely mimics cell-cell contact. Moreover, they rely on synthetic polymer chemistries and cannot be readily adapted to the wide variety of natural hydrogels (collagen, fibrin, gelatin, Matrigel, etc.) most commonly used as extracellular matrix mimics. While rare reports of magnetically actuated natural hydrogels exist,[30,31] their ability to generate forces across the full biologically relevant range (from pN to μN), as well as their functional impact on any specific biological tissue, has not yet been assessed, to our knowledge.

We have developed a magnetic extracellular matrix and custom-built actuation platform that can generate modular, programmable, and tunable deformation within multicellular systems. We test this platform as an active substrate for skeletal muscle, an important tissue that is responsible for all voluntary motion in our bodies and is highly adaptive to mechanical signaling.[32,33] Our study shows that we can control the directional fusion of myoblasts into aligned fibers through dynamic mechanical stimulation. Furthermore, we develop robust computational tools for tracking substrate deformation in response to muscle contraction. Our computational analysis clearly demonstrates that mechanically programmed anisotropy in muscle coordinates tissue-wide synchrony of contractile twitch. Precisely controlling muscle fiber alignment and synchronous contraction is of significant importance in tissue engineering applications ranging from medicine to robotics.[34–37] These results indicate that our technology can be used to improve the ease and efficiency of established methods to pattern muscle morphology. Beyond muscle, this study sets the stage for deploying actuating extracellular matrices as devices to map and modulate mechanical signaling within a range of multicellular tissues, enabling user-defined control of adaptive mechanobiological processes.

RESULTS

Design and fabrication of magnetically actuated extracellular matrices

Magnetically controlled soft actuators, composed of iron nano- and microparticles embedded within flexible materials, have been of significant interest in soft robotics in recent years, as they enable non-contact control of actuation with high spatiotemporal resolution.[38,39] Inspired by this approach, we mixed iron microparticles with poly(dimethyl siloxane) (PDMS) to form a sheet of magnetic silicone. We then formed magnetic silicone microparticles from this sheet and sandwiched these microparticles between two layers of a fibrin hydrogel in a cell culture plate (Figure 1A). Compression testing of the hydrogels revealed an average elastic modulus of 18.4 ± 3.4 kPa for magnetic fibrin and of 19.1 ± 4.4 kPa for non-magnetic fibrin, confirming that there was no significant difference between groups (Figure 1B). These results indicated that the mechanical properties of the magnetic fibrin were likely suitable for cell culture.[40] Future studies that explore the rheological properties of magnetic fibrin could further clarify whether adhered cells sense significant stiffness differences between magnetic and non-magnetic fibrin.[41]

To dynamically control the movement of the resultant composite magnetic extracellular matrix, we constructed a custom linear actuator to move a permanent magnet under the plate with precisely controllable speed (Figure 1C; Video S1). Fluorescent beads embedded within the hydrogel were used to track matrix deformation in response to the magnetically guided movement of a microparticle, showing that deformation of the hydrogel was highest in the region closest to the microparticle (Figure 1D; Video S2). We thus embedded an array of magnetic microparticles within the fibrin hydrogels and optimized microparticle spacing to generate a more uniform deformation gradient in the region between adjacent microparticles (Figure S1A).

We tested the impact of a variety of magnetic stimulation parameters on the platform to showcase the versatility of this system. For example, we observed that for a fixed value of permanent magnet strength and microparticle composition and size, hydrogel deformation is dependent on the distance between the magnet and the hydrogel (Figures 1E and S1B; Videos S3, S4, and S5). We also tested the impact of magnet speed and orientation on the deformation of the hydrogel, demonstrating that reducing the speed of the magnet or rotating the magnet from 0° to 45° or 90° shifted the rate and direction of microparticle movement, respectively (Figures S1C–S1G).

These analyses demonstrated the ability of our device to enable precisely controllable magnetic matrix actuation (MagMA), motivating studying the impact of dynamic mechanical stimulation on biological tissues. As a proof-of-concept demonstration, we chose to test the impact of our MagMA hydrogel platform on muscle, a highly mechanically adaptive tissue that controls all voluntary movement in our bodies.[32,33]

Effect of dynamic mechanical stimulation on myoblast proliferation, fusion, and maturation

Optogenetic C2C12 mouse myoblasts[42] were seeded on MagMA hydrogels and were maintained in a growth medium until they generated a confluent monolayer of cells after 24 h. They were transitioned to a differentiation medium after 48 h (day 0). Our previous studies have shown that exercise training (low-frequency stimulation with 470 nm light for 30 min/day over 10 days) can dramatically improve muscle force by ~3×.[43] We thus implemented a similar dynamic mechanical stimulation protocol to test whether mechanical training alone could similarly modulate muscle maturation (Figure 2A). We chose magnetic stimulation parameters that generated deformations similar to those generated by contractile C2C12-derived muscle during exercise (~1%–4% strain; Figure 1E), as reported in previously published studies.[42,44,45]

We fixed and stained muscle tissues with a cell nuclei marker (DAPI) to assess the impact of dynamic mechanical stimulation on myoblast proliferation and fusion into multinucleated fibers. We observed no significant difference between the total number of nuclei in control and stimulated groups, indicating that our dynamic mechanical stimulation protocol had no impact on cell

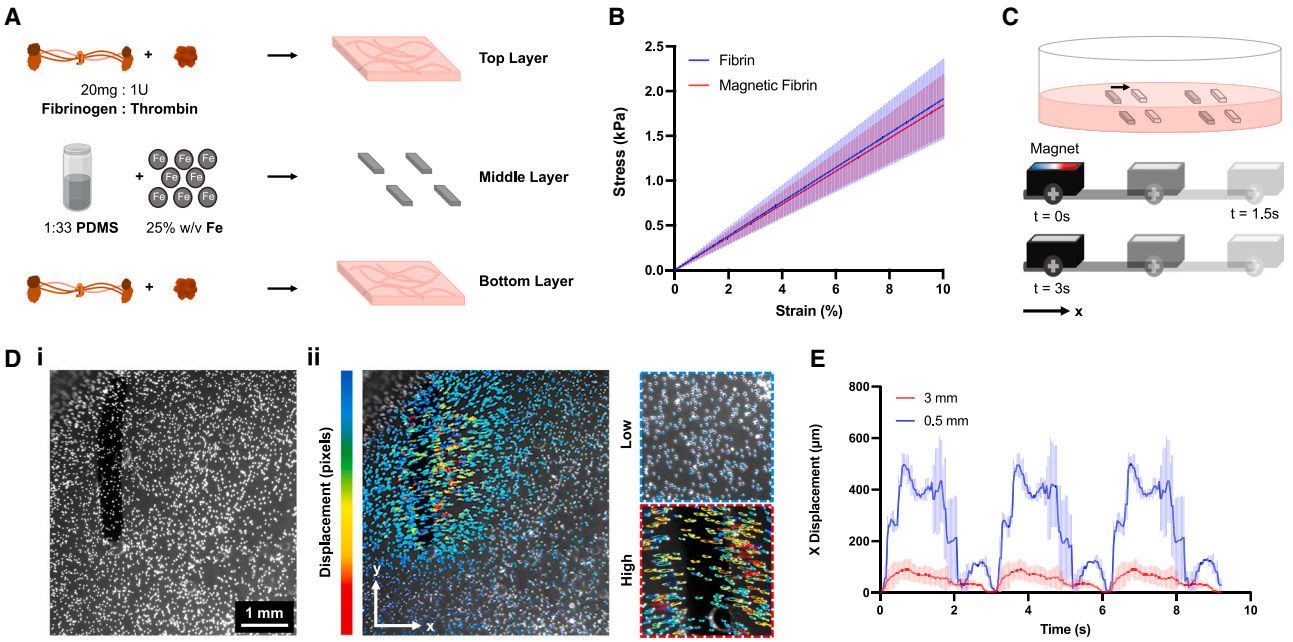

Figure 1. Design and fabrication of extracellular matrices enabling magnetic matrix actuation (MagMA)

(A) Schematic of magnetic matrix fabrication. An array of iron-loaded microparticles (500 × 2,000 μm) is sandwiched between two layers of a fibrin extracellular matrix-mimicking hydrogel.

(B) Stress-strain curve for magnetic and non-magnetic fibrin, showing no statistically significant difference in elastic modulus between 0% and 10% strain. n = 4 per group. Error bars indicate standard deviation from the mean.

(C) Schematic of actuation mechanism. Magnet moves parallel to the x axis (Video S1). Controlling the direction and speed of a permanent magnet drives actuation of the hydrogel (Figure S1).

(D) Fluorescent beads embedded in the magnetic hydrogel (i) enable tracking hydrogel displacement (ii). Left: matrix displacement is highest in gel regions closest to the microparticle (Video S2). Right: magnified images of regions of low and high displacement, representing regions far from and near to the magnetic microparticle, respectively.

(E) Experimental data plotting x-direction gel displacement as a function of distance between the magnet and the hydrogel (distance = 0.5 and 3 mm), n = 3 per group (Videos S3, S4, and S5). Error bars indicate standard deviation from the mean.

proliferation. We also followed established methods to perform an analysis of circularity,[45–47] as near-spherical cells (circularity ~1) would indicate no fusion has occurred and reduced circularity would indicate nuclei have fused and elongated. We noted that substrate actuation did significantly reduce circularity, indicating enhanced fusion of myoblasts into multinucleated fibers (Figure 2B). Further morphological analysis revealed that both control and stimulated fibers grow significantly in length over time, but no significant difference in fiber length or width was observed between experimental groups on day 5 or 8 (Figure 2C).

Dynamic mechanical programming of muscle fiber alignment

Global fiber alignment is critical to native muscle architecture, as tissue-wide actuation can only be achieved by independent fibers twitching simultaneously and in the same direction.[48] In the context of regenerative medicine, manufacturing engineered muscle that matches the form of native tissue is critical to *in vivo* implantation and integration.[49] Likewise, for applications in high-throughput drug testing, quantitatively comparing the contractile force generated by muscle in physiological and pathological states requires reproducible fabrication of highly aligned constructs.[50] Programming muscle anisotropy is perhaps most relevant in applications of muscle as a functional actuator in robots, where force output and directionality must be tightly controlled to precisely regulate device function.[44,45,48] There is thus a significant need, across diverse application areas, for methods to efficiently and effectively program alignment within muscle.

Existing techniques to align muscle fibers control the fusion of neighboring myoblasts through microscale geometric and biochemical cues, chronic passive stretch, and even acoustically guided cell positioning.[51–53] Microscale patterning and acoustic positioning require complex fabrication techniques that must be modified for each desired alignment pattern and can only be deployed at the time of tissue assembly. Passive stretch, likewise, is chronically present throughout culture and generates non-uniform deformation gradients that cannot be spatially modulated within the tissue.[28] There is thus a significant need for a technique enabling dynamically spatiotemporal control of the orientation of muscle fibers within engineered tissues. Our MagMA platform allows changing the rate, intensity, and angle of deformation by changing the magnetic field orientation and strength (Figures 1 and S1), providing a potential solution to this outstanding challenge in guiding muscle alignment.

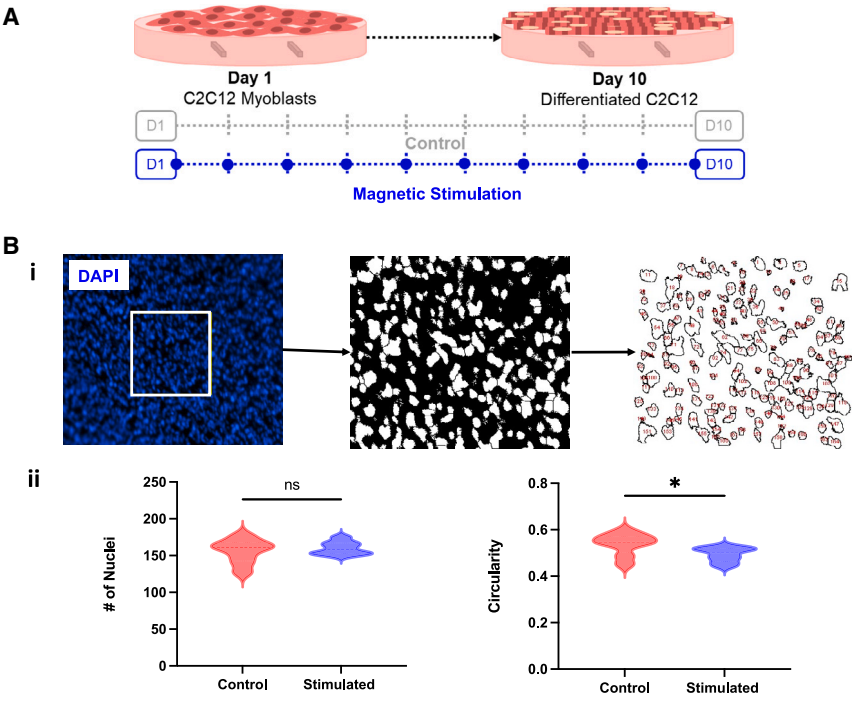

Figure 2. Effect of dynamic mechanical stimulation on myoblast proliferation, fusion, and maturation

(A) Schematic of experimental design and timeline.

(B) (i) Left: DAPI image depicting cell nuclei at 10× magnification. 100,000 μm^2 region of interest (ROI) selected and analyzed for each of the images. Middle: image thresholded and watershed to segment connected nuclei. Right: "analyze particles" feature in ImageJ used to obtain nuclei count and circularity. (ii) Violin plots depicting nuclei number (left) and circularity (right) show that magnetic stimulation has no impact on cell proliferation but does have an impact on nuclei fusion and spreading. Unpaired t test, n = 4 per group, $^*p < 0.05$.

(C) (i) Representative image showing measurement method for calculating fiber length (top) and fiber width (bottom). Optogenetic ChR2 ion channels in the cell membrane are tagged with a tdTomato red fluorescent tag, enabling fiber visualization. (ii) Violin plots of average fiber length and width at days 5 and 8 between experimental groups. Unpaired t test, n = 4 per group, $^*p < 0.05$.

Our prior studies corroborate previous observations by others that chronic mechanical stretch enhances fiber alignment in engineered muscle and that disrupting global alignment can have a significant negative impact on contractile force.[42,48] The MagMA platform allowed us to assess, for the first time, the impact of a short period of dynamic mechanical actuation on fiber alignment. Following the stimulation regimen outlined in Figure 2A, we fixed our muscle tissues and imaged a fluorescent marker of the optogenetic membrane ion channel (ChR2). We observed that muscle cultured on stimulated MagMA hydrogels appeared to be globally aligned, in contrast to control muscle cultured on non-stimulated MagMA hydrogels (Figure 3A). We used a fast Fourier transform (FFT) image analysis technique to quantify differences in local and global alignment across control and magnetically stimulated groups. These results corroborated our visual analyses, showing that fibers in mechanically stimulated tissues were significantly more likely to align parallel to the direction of magnet movement (defined as 0°) (Figure 3B). By contrast, fibers in control tissues did not demonstrate statistically significant global alignment and were relatively evenly distributed across a wide range of angles (Figures 3C and 3D).

Mechanically programmed alignment coordinates synchronous global contraction

We have previously shown that the contraction of optogenetic muscle can be controlled with a 470 nm light stimulus.[42] By leveraging our established techniques, we optically stimulated muscle tissues on day 10 of culture and recorded videos of contraction. Quantitative comparison of motility in complex non-homogeneous biological tissues is a challenging task, motivating the development of novel computational frameworks to perform this analysis in a robust, reproducible, and automated manner.[54] We thus developed an open-source automated image processing tool to map the deformation of skeletal muscle in response to light stimulation. This tool helped us make clear quantitative comparisons between experimental groups.

Optical stimulation of engineered muscle generated globally coordinated twitch deformation in mechanically programmed tissues, while control tissues displayed asynchronous and arrhythmic contraction (Figures 4A–4C; Videos S6, S7, S8, and S9), indicating that improved global fiber alignment had an observable downstream impact on function. To better visualize and quantify differences in the global synchrony of muscle contractility, we mapped deformation into normal strain along the x axis (0°, parallel to magnet movement) and visualized strain

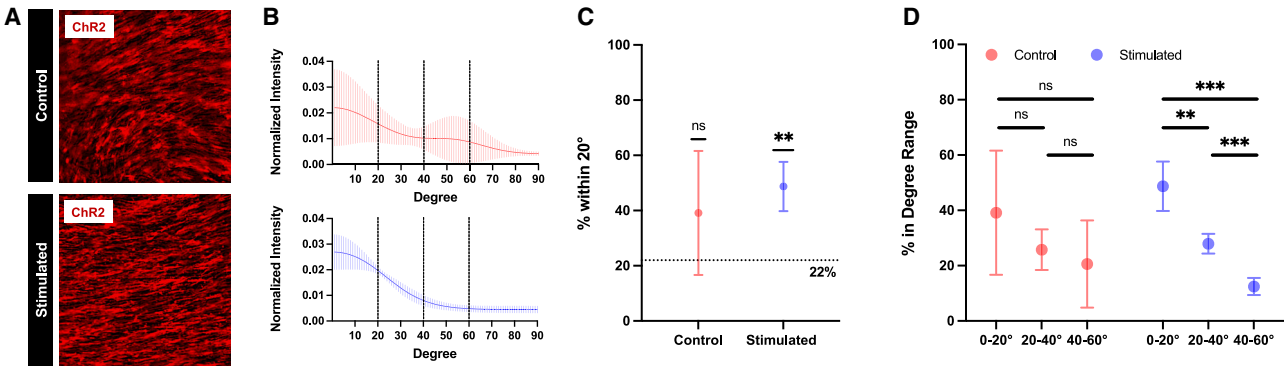

Figure 3. Mechanically programmed muscle fiber alignment

(A) Representative images of fibers between two magnetic microparticles within a well for control (top) and stimulated (bottom) groups.

(B) Histogram showing fiber alignment as a function of degree deviation from 0°, parallel to the direction of magnet movement for control (top, red) and stimulated (bottom, blue) groups.

(C) Comparison of percentage of fibers that fall within 20° of desired alignment (0°) for control and stimulated groups. If fibers were randomly aligned, they would be evenly distributed across 0°–90°, and one would expect ~22% of fibers to fall within this range. In the stimulated group, there is a significantly larger percentage of fibers that fall within 20° of desired angle, indicating directed global alignment. One sample t test comparing to hypothetical mean of 22%, n = 4 per group, **p < 0.01. Importantly, both control and stimulated groups are significantly different from 100%, i.e., perfect alignment, indicating a future need to optimize stimulation parameters to improve alignment efficiency. Error bars indicate standard deviation from the mean.

(D) Comparison of percentage of fibers that fall within 0°–20°, 20°–40°, and 40°–60° deviation from desired angle (0°) shows that, in control groups, fibers are fairly evenly distributed across a range of angles, whereas the large majority of fibers in stimulated groups fall within 0°–20°. Unpaired t test, n = 4 per group, **p < 0.01, ***p < 0.001. Error bars indicate standard deviation from the mean.

across multiple regions within each sample (Videos S10 and S11). Plotting the subdomain-averaged strain of selected regions within the image, including regions closer to and farther away from the magnetic microparticles, enabled tracking the direction and timing of the twitch in response to three sequential light pulses (Figure 4C). Our analyses revealed that, across multiple samples and multiple regions within each sample, tissues mechanically programmed via MagMA hydrogels demonstrated a coordinated twitch, while control tissues were asynchronously contractile. These data indicate that in the absence of global alignment, muscle fibers deform the substrate in multiple different directions during contraction. The amount of tissue displacement generated along a given direction is proportional to the number of fibers oriented at that angle. Non-uniform distribution of fibers at various angles generates non-uniform spatial forces that seem to change the resultant relaxation properties of the tissue, thus reducing twitch synchrony. Overall, our functional assays corroborate the observation that the MagMA platform mechanically programs anisotropy of both form and function in engineered muscle.

DISCUSSION

Soft actuating substrates for cell culture are of significant interest for actively controlling mechanical signaling within tissues. In the context of skeletal muscle, the ability to simply and dynamically program fiber alignment is important for tissue engineering applications ranging from regenerative medicine to biohybrid robotics. Here, we show that MagMA-driven dynamic mechanical stimulation controls the directionality of fusion between neighboring myoblasts into mature muscle fibers, thus robustly programming global alignment and coordinated contractility.

We have observed that myoblasts cultured on soft gels will differentiate into locally aligned fibers within small regions (~100s of μm), likely because of traction forces imposed by single cells on their neighbors. However, this passive culture technique does not program the global alignment required to generate coordinated contraction in the mm- and cm-scale tissues relevant for real-world applications. Several prior studies have demonstrated techniques for globally aligning muscle fibers within engineered tissues via microscale geometric cues, biochemical patterns, passive mechanical stretch, and acoustically guided cell positioning.[51,52,55–57] While these techniques are effective, they can only be deployed at the time of cell seeding and are not designed to be dynamically changed or spatially controlled over time. For example, micropatterned substrates must be redesigned and manufactured for each desired alignment pattern. By contrast, the MagMA platform enables dynamically tuning stimulation parameters (such as magnet orientation angle) to change alignment patterns without altering the substrate fabrication process. Moreover, MagMA is dynamically deployable and could be used, in the future, to program fiber orientation at any point prior to terminal differentiation of cells.

Our actuating extracellular matrices allowed us to decouple the mechanical and biochemical effects of exercise by independently studying the effects of dynamic mechanical stimulation alone on fiber formation and maturation. In prior studies, we and others have shown that exercise (30 min/day, 10 days) increases muscle force by ~3× and that combining exercise with chronic mechanical stretch synergistically increased force by an additional 50%.[42,58] These functional improvements were correlated with upregulation of key myogenic regulatory factors.[43,58] Our previous studies indicate that exercise impacts the size and maturation of muscle fibers, whereas this study

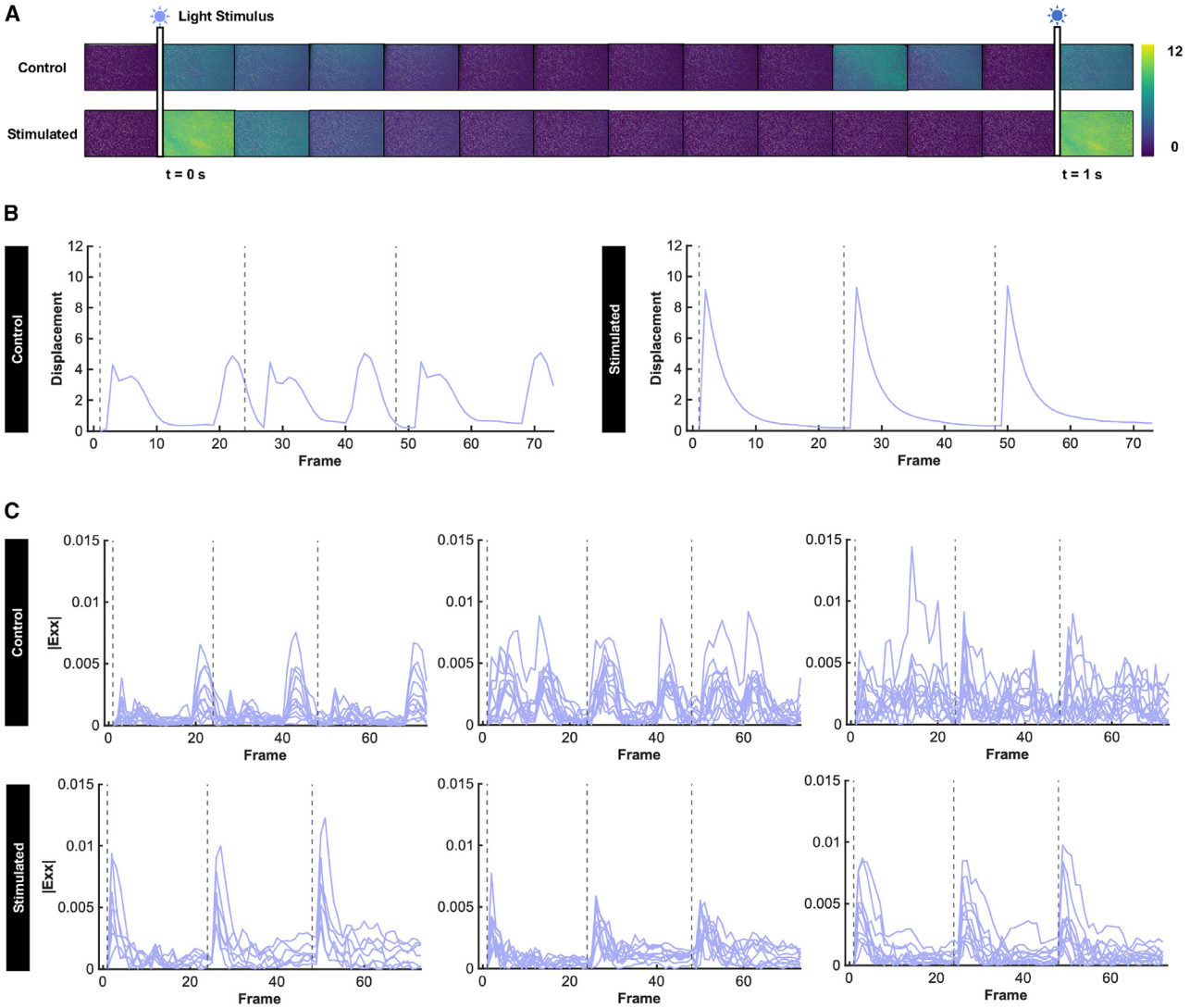

Figure 4. Mechanically programmed alignment coordinates synchronous global contraction

(A) Timelapse images showing total displacement of fibers in response to a light stimulus for representative sample from control (top) and stimulated (bottom) groups (Videos S6, S7, S8, and S9).

(B) Plotting total displacement data in representative control (left) and stimulated (right) samples indicates paced global contraction is only observed in the stimulated sample.

(C) Plots of normal strain along the x axis for multiple regions within three control (top) and three stimulated (bottom) samples showing that global synchrony of twitch along 0° is only observed in the stimulated group (Videos S10 and S11). Dashed lines indicate a light stimulus at 1 Hz. Video acquired at ~25 fps.

demonstrates that dynamic mechanical stimulation in the absence of exercise modulates myoblast fusion and muscle fiber alignment.

Mechanical stimulation alone is thus not equivalent to exercise, providing a potential explanation for the previously observed synergistic increases in muscle force in response to combined biochemical and mechanical stimulation. These results motivate future studies using MagMA in combination with other modes of stimulation. It is important to note that while we observed no impact of mechanical stimulation on proliferation rates, others have observed actuation-mediated modulation of myoblast proliferation after longer stimulation periods (~5–17 h).[59] These differing results indicate that varying the duration, magnitude, and frequency of mechanical stimulation can significantly change functional outcomes and could be used to further tune muscle mechanobiological processes beyond fiber alignment in future studies.

Interestingly, we have found that tension cues do not need to be chronically present throughout maturation, as was previously assumed by muscle researchers in both *in vitro* and *in vivo* contexts.[42,44,45,48,50,56,57,60,61] Rather, a short daily regimen of dynamic mechanical stimulation (30 min/day, 10 days) can sufficiently program long-lasting functional anisotropy in muscle. This is an important advantage of our MagMA platform, as it

allows on/off control of dynamic mechanical stimulation, allowing researchers to study the separate and combined impact of biochemical, electrical, and mechanical stimuli on multicellular systems during key periods of assembly and maturation.

Our study is a proof-of-concept demonstration that modulating intercellular forces in skeletal muscle during differentiation can dynamically program tissue anisotropy. It is important to note that we have not optimized how modulating system parameters impacts muscle morphology or function. Future work to improve the efficiency and complexity of patterned alignment will leverage our platform's flexibility in modulating the frequency, duration, directionality, and timeline of mechanical stimulation (Figures 1 and S1).

Beyond muscle, magnetically actuating hydrogels address a key need in tissue engineering by enabling researchers to modulate forces within tissues and study the impact on architecture and function. The rate, degree, and angle of gel deformation can be simply tuned by changing the size and distribution of the magnetic microparticles or the orientation of the magnet. Moreover, this platform can be readily adapted to a variety of natural and synthetic hydrogel chemistries that are well suited to a range of cell types. We anticipate that actuating extracellular matrices will be useful devices for programming microscale hierarchy in engineered muscle, and that this platform will drive a broad range of fundamental and translational studies of mechanobiology, regenerative medicine, and biohybrid robotics.

EXPERIMENTAL PROCEDURES

Resource availability

Lead contact

Further information and requests for resources and reagents should be directed to and will be fulfilled by the lead contact, Ritu Raman (ritur@mit.edu).

Materials availability

This study did not generate new unique reagents.

Data and code availability

- All data needed to evaluate the conclusions in the paper are present in the paper and/or the supplemental information.
- Our original code is provided on GitHub under an open-source MIT License as a supplement to this work: https://github.com/HibaKob/Raman_Manuscript_2023.
- Any additional information required to reanalyze the data reported in this paper is available from the lead contact upon request.

Fabrication and mechanical characterization of magnetic extracellular matrices

To fabricate 5 g of the 25% w/w iron microparticle-loaded PDMS (1:33 monomer:crosslinker ratio), we added 3.64 g Sylgard 184 Base, 0.11 g curing agent, and 1.25 g 4 μm diameter iron microparticles (US Research Nanomaterials) to a weigh boat and mixed thoroughly via manual stirring. Following de-gassing in a vacuum desiccator for 10 min, we poured the mixture into a flat, rectangular mold made from polylactic acid and cured it in a 100°C oven overnight. To construct magnetic hydrogels, we prepared an 8 mg mL^{-1} solution of fibrinogen (Thermo Scientific) in DMEM (Corning) supplemented with 1 mg mL^{-1} aminocaproic acid (Sigma Aldrich). We mixed 0.4 U per mg fibrinogen of thrombin (Sigma Aldrich) with the fibrinogen solution just prior to pipetting into a 24-well plate (200 μL per well) and incubated at 37°C for 1 h. We used a razor to cut four 500 × 2,000 μm pieces of iron microparticle-loaded PDMS. Using forceps, we arranged the magnetic microparticles into an array on the gel, with adjacent microparticles spaced 2,000 μm apart. A second layer of fibrin (400 μL) was pipetted over the array and incubated at 37°C overnight. After all experimental data were collected, we performed compression testing using a texture analyzer to obtain stress-strain curves and measure the Young's modulus of our magnetic and non-magnetic hydrogels.

Design and development of magnetic actuation platform

We customized a commercially available linear actuator (Actuonix L16R Servo) to mechanically stimulate our magnetic hydrogel by affixing a permanent neodymium magnet to one end of the actuator with a custom 3D-printed holder. Arduino code was used to program the desired servo actuation parameters.

Muscle differentiation, mechanical stimulation, and optical stimulation

Optogenetic mouse myoblast cells (C2C12 engineered to express a mutant variant of the 470 nm blue light-sensitive ion channel, Channelrhodopsin [ChR2(H134R)]) labeled with a tdTomato tag[42] were expanded in GM+: DMEM with 4.5 g L^{-1} glucose, L-glutamine, and sodium pyruvate (Corning) supplemented with 10% fetal bovine serum (Lonza) and 1 mg mL^{-1} aminocaproic acid (Sigma Aldrich). Cells were trypsinized with TrypLE (Gibco), counted with trypan blue (Gibco), and seeded atop the fibrin hydrogel at a concentration of 100,000 cells per well. The cells continued to proliferate in GM+ for 48 h, at which point the media were switched to DM++: DMEM (Corning) supplemented with 10% horse serum (Thermo Scientific), 1 mg mL^{-1} aminocaproic acid (Sigma Aldrich), and 50 ng mL^{-1} human insulin-like growth factor 1 (Sigma Aldrich).

To mechanically stimulate the cells, the well plate containing the cell-seeded magnetic hydrogel was held in place above the linear actuator such that magnet actuation deformed the substrate. A daily exercise regime of low-frequency stimulation (0.33 cycles per s for 30 min per well) was implemented over 10 days. On the last day, global muscle contraction of both experimental groups was characterized in response to 1 Hz light stimulation with a 470 nm optical fiber (ThorLabs).

Immunohistochemical staining and fluorescence imaging

After live-cell experiments were completed, tissues were fixed and stained to visualize cell nuclei and fiber formation. We used 4% paraformaldehyde in phosphate-buffered saline (PBS) to fix our tissue for 15 min, followed by a PBS rinse. We then permeabilized the tissue for 15 min using 0.5% Triton X-100 (Thermo Scientific) in PBS and blocked using 5% bovine serum albumin in PBS for 60 min, washing with 1 mL PBS in between each step. Finally, tissues were stained with NucBlue (Thermo Scientific) for 15 min and washed with PBS prior to imaging. Fluorescence imaging was performed using an EVOS fluorescence microscope. A DAPI stain was used to visualize nuclear DNA and aid with characterization of cell nuclei. Optogenetic ion channels in the muscle cell membrane were tagged with a tdTomato label to enable quantification of global fiber alignment.[42]

Image processing and statistical analysis

ImageJ (https://imagej.nih.gov/ij/download.html) and Nikon Clarify.ai (https://www.microscope.healthcare.nikon.com/products/software/nis-elements/nis-ai-1) were used for all image processing. Brightness and contrast were adjusted to better visualize representative images and then cropped to eliminate out-of-focus regions. Muscle fiber length and width were measured on days 5 and 8 using ImageJ's segmented line and measure tools, taking into account the appropriate pixel-to-μm conversion. Nuclei density was quantified by cropping a 100,000 μm^2 region on each image, thresholding to convert image to black and white, watershedding to separate any combined nuclei, and then using the analyze particles tool to obtain the total number and circularity of the nuclei. We used ImageJ's Directionality plugin to quantify differences in local and global alignment across control and magnetically stimulated groups. FFT of the images yields 2D power spectra, which were then analyzed in polar coordinates to measure the power in each angle.

GraphPad Prism (https://www.graphpad.com/) was used to compile, analyze, and visualize all data. Statistical analysis used for each figure are outlined in the figure captions.

Optical tracking

To characterize global muscle contraction in response to light stimulation, we implemented a modified version of a full-field displacement and strain tracking

code that was originally developed for use in cardiac microtissue.[62] Our open-source code is written in Python and is based on the OpenCV[63] implementation of the Lucas-Kanade sparse optical flow algorithm.[64] In this approach, tracking points distributed throughout the domain are automatically identified based on the Shi-Tomasi "good features to track" algorithm,[65] which depends on the natural contrast and texture inherent to optical images of the muscle sheets. The original code (https://github.com/HibaKob/MicroBundleCompute) required two key customizations for these data: (1) manual specification of the region of interest via manually tracing the muscle domain in a relaxed state in ImageJ, and (2) a custom preprocessing step where we automatically identified the frames where optical stimulation was performed within each movie to skip during tracking. The preprocessing step is essential, as a substantial and transient change in exposure between frames would degrade the performance of the optical flow algorithm.

By tracking automatically identified markers across consecutive frames, we were able to compute full-field displacements, subdomain-averaged strains, and strain-derived metrics to quantitatively capture the mechanical behavior of the muscle sheets. Consistent with our previous approaches to analyzing cardiac microtissue (2), we opted to output subdomain-averaged strains with respect to time as a key metric. Specifically, we divided the muscle region into a grid of equal aspect ratio boxes (Video S8) of size 100 pixels (except for the control4 example, where the tile dimension is 80 pixels) and then computed, within each box, the best-fit deformation gradient for mapping the markers between their relaxed and contracted positions. This best-fit deformation gradient was then used to compute the Green-Lagrangian strain tensor, which captures the deformation behavior of these tissue. The modified version of our tracking code is provided on GitHub under an open-source MIT License as a supplement to this work: https://github.com/HibaKob/Raman_Manuscript_2023.

SUPPLEMENTAL INFORMATION

Supplemental information can be found online at https://doi.org/10.1016/j.device.2023.100097.

ACKNOWLEDGMENTS

The authors would like to thank Nicolas Castro, Naomi Lynch, and Elizabeth Calle for technical discussions. This work was supported in part by the US DoD Army Research Office Early Career Program (awarded to R.R.), the NSF CAREER program (awarded to R.R.), the NEC Corporation Fund (awarded to R.R.), and the NSF Graduate Research Fellowship Program (awarded to B.R. and A.B.).

AUTHOR CONTRIBUTIONS

Conceptualization, R.R.; methodology, B.R., A.B., T.S., H.K., E.L., and R.R.; software, H.K. and E.L.; validation, E.L. and R.R.; formal analysis, B.R., A.B., T.S., H.K., E.L., and R.R.; investigation, B.R., A.B., T.S., S.K., and K.S.; resources, E.L. and R.R.; data curation, B.R., A.B., T.S., H.K., E.L., and R.R.; writing – original draft, B.R., A.B., T.S., H.K., E.L., and R.R.; writing – review & editing, E.L. and R.R.; visualization, B.R., A.B., T.S., H.K., E.L., and R.R.; supervision, E.L. and R.R.; project administration, R.R.; funding acquisition, E.L. and R.R.

DECLARATION OF INTERESTS

R.R. is a member of the *Device* advisory board.

Received: July 3, 2023
Revised: August 11, 2023
Accepted: September 11, 2023
Published: October 20, 2023

REFERENCES

1. Aydin, O., Passaro, A.P., Raman, R., Spellicy, S.E., Weinberg, R.P., Kamm, R.D., Sample, M., Truskey, G.A., Zartman, J., Dar, R.D., et al. (2022). Principles for the design of multicellular engineered living systems. APL Bioeng. *6*, 010903. https://doi.org/10.1063/5.0076635.
2. Dagdeviren, C., Ramadi, K.B., Joe, P., Spencer, K., Schwerdt, H.N., Shimazu, H., Delcasso, S., Amemori, K.I., Nunez-lopez, C., Graybiel, A.M., et al. (2018). Miniaturized neural system for chronic, local intracerebral drug delivery. Sci. Transl. Med. *10*, eaan2742.
3. Raman, R., Rousseau, E.B., Wade, M., Tong, A., Cotler, M.J., Kuang, J., Lugo, A.A., Zhang, E., Graybiel, A.M., White, F.M., et al. (2020). Platform for micro-invasive membrane-free biochemical sampling of brain interstitial fluid. Sci. Adv. *6*, eabb0657.
4. Style, R.W., Boltyanskiy, R., German, G.K., Hyland, C., MacMinn, C.W., Mertz, A.F., Wilen, L.A., Xu, Y., and Dufresne, E.R. (2014). Traction force microscopy in physics and biology. Soft Matter *10*, 4047–4055. https://doi.org/10.1039/C4SM00264D.
5. Shiwarski, D.J., Tashman, J.W., Tsamis, A., Bliley, J.M., Blundon, M.A., Aranda-Michel, E., Jallerat, Q., Szymanski, J.M., McCartney, B.M., and Feinberg, A.W. (2020). Fibronectin-based nanomechanical biosensors to map 3D surface strains in live cells and tissue. Nat. Commun. *11*, 5883. https://doi.org/10.1038/s41467-020-19659-z.
6. Kamble, H., Barton, M.J., Jun, M., Park, S., and Nguyen, N.-T. (2016). Cell stretching devices as research tools: engineering and biological considerations. Lab Chip *16*, 3193–3203. https://doi.org/10.1039/C6LC00607H.
7. Moreno-Mateos, M.A., Gonzalez-Rico, J., Nunez-Sardinha, E., Gomez-Cruz, C., Lopez-Donaire, M.L., Lucarini, S., Arias, A., Muñoz-Barrutia, A., Velasco, D., and Garcia-Gonzalez, D. (2022). Magneto-mechanical system to reproduce and quantify complex strain patterns in biological materials. Appl. Mater. Today *27*, 101437. https://doi.org/10.1016/j.apmt.2022.101437.
8. Rangarajan, S., Madden, L., and Bursac, N. (2014). Use of Flow, Electrical, and Mechanical Stimulation to Promote Engineering of Striated Muscles. Ann. Biomed. Eng. *42*, 1391–1405. https://doi.org/10.1007/s10439-013-0966-4.
9. Hussien, A.A., Niederoest, B., Bollhalder, M., Goedecke, N., and Snedeker, J.G. (2023). The Stiffness-Sensitive Transcriptome of Human Tendon Stromal Cells. Adv. Healthcare Mater. *12*, e2101216. https://doi.org/10.1002/adhm.202101216.
10. Shou, Y., Teo, X.Y., Wu, K.Z., Bai, B., Kumar, A.R.K., Low, J., Le, Z., and Tay, A. (2023). Dynamic Stimulations with Bioengineered Extracellular Matrix-Mimicking Hydrogels for Mechano Cell Reprogramming and Therapy. Adv. Sci. *10*, e2300670. https://doi.org/10.1002/advs.202300670.
11. Puetzer, J.L., and Bonassar, L.J. (2016). Physiologically Distributed Loading Patterns Drive the Formation of Zonally Organized Collagen Structures in Tissue Engineered Meniscus. Tissue Eng. *22*, 907–916. https://doi.org/10.1089/ten.tea.2015.0519.
12. Huh, D., Matthews, B.D., Mammoto, A., Montoya-Zavala, M., Hsin, H.Y., and Ingber, D.E. (2010). Reconstituting organ-level lung functions on a chip. Science *328*, 1662–1668. https://doi.org/10.1126/science.1188302.
13. Raman, R., and Bashir, R. (2017). Biomimicry, Biofabrication, and Biohybrid Systems: The Emergence and Evolution of Biological Design. Adv. Healthcare Mater. *6*, 1700496. https://doi.org/10.1002/adhm.201700496.
14. Raman, R., and Langer, R. (2020). Biohybrid Design Gets Personal: New Materials for Patient-Specific Therapy. Adv. Mater. *32*, e1901969. https://doi.org/10.1002/adma.201901969.
15. Breger, J.C., Yoon, C., Xiao, R., Kwag, H.R., Wang, M.O., Fisher, J.P., Nguyen, T.D., and Gracias, D.H. (2015). Self-folding thermo-magnetically responsive soft microgrippers. ACS Appl. Mater. Interfaces *7*, 3398–3405. https://doi.org/10.1021/am508621s.
16. Zhang, S., Bellinger, A.M., Glettig, D.L., Barman, R., Lee, Y.A.L., Zhu, J., Cleveland, C., Montgomery, V.A., Gu, L., Nash, L.D., et al. (2015). A pH-responsive supramolecular polymer gel as an enteric elastomer for use in gastric devices. Nat. Mater. *14*, 1065–1071. https://doi.org/10.1038/nmat4355.

17. Liu, J., Pang, Y., Zhang, S., Cleveland, C., Yin, X., Booth, L., Lin, J., Lucy Lee, Y.A., Mazdiyasni, H., Saxton, S., et al. (2017). Triggerable tough hydrogels for gastric resident dosage forms. Nat. Commun. *8*, 124–129. https://doi.org/10.1038/s41467-017-00144-z.

18. Rapp, T.L., and Deforest, C.A. (2020). Visible Light-Responsive Dynamic Biomaterials : Going Deeper and Triggering More. Adv. Healthcare Mater. *9*, e1901553. https://doi.org/10.1002/adhm.201901553.

19. Raman, R., Hua, T., Gwynne, D., Collins, J., Tamang, S., Soares, V., Esfandiary, T., Zhou, J., Pajovic, S., Hayward, A., et al. (2020). Light-degradable hydrogels as dynamic triggers in gastrointestinal applications. Sci. Adv. *6*, eaay0065.

20. Haider, H., Yang, C.H., Zheng, W.J., Yang, J.H., Wang, M.X., Yang, S., Zrínyi, M., Osada, Y., Suo, Z., Zhang, Q., et al. (2015). Exceptionally tough and notch-insensitive magnetic hydrogels. Soft Matter *11*, 8253–8261. https://doi.org/10.1039/C5SM01487E.

21. Batalov, I., Stevens, K.R., and DeForest, C.A. (2021). Photopatterned biomolecule immobilization to guide three-dimensional cell fate in natural protein-based hydrogels. Proc. Natl. Acad. Sci. USA *118*, e2014194118. https://doi.org/10.1073/pnas.2014194118.

22. Liu, L., Shadish, J.A., Arakawa, C.K., Shi, K., Davis, J., and DeForest, C.A. (2018). Cyclic Stiffness Modulation of Cell-Laden Protein-Polymer Hydrogels in Response to User-Specified Stimuli Including Light. Adv. Biosyst. *2*, 1800240. https://doi.org/10.1002/adbi.201800240.

23. Shou, Y., Teo, X.Y., Li, X., Zhicheng, L., Liu, L., Sun, X., Jonhson, W., Ding, J., Lim, C.T., and Tay, A. (2023). Dynamic Magneto-Softening of 3D Hydrogel Reverses Malignant Transformation of Cancer Cells and Enhances Drug Efficacy. ACS Nano *17*, 2851–2867. https://doi.org/10.1021/acsnano.2c11278.

24. Sutton, A., Shirman, T., Timonen, J.V.I., England, G.T., Kim, P., Kolle, M., Ferrante, T., Zarzar, L.D., Strong, E., and Aizenberg, J. (2017). Photothermally triggered actuation of hybrid materials as a new platform for in vitro cell manipulation. Nat. Commun. *8*, 14700. https://doi.org/10.1038/ncomms14700.

25. Özkale, B., Lou, J., Özelçi, E., Elosegui-Artola, A., Tringides, C.M., Mao, A.S., Sakar, M.S., and Mooney, D.J. (2022). Actuated 3D microgels for single cell mechanobiology. Lab Chip *22*, 1962–1970. https://doi.org/10.1039/D2LC00203E.

26. Chandorkar, Y., Castro Nava, A., Schweizerhof, S., Van Dongen, M., Haraszti, T., Köhler, J., Zhang, H., Windoffer, R., Mourran, A., Möller, M., and De Laporte, L. (2019). Cellular responses to beating hydrogels to investigate mechanotransduction. Nat. Commun. *10*, 4027. https://doi.org/10.1038/s41467-019-11475-4.

27. Roy, A., Zhang, Z., Eiken, M.K., Shi, A., Pena-Francesch, A., and Loebel, C. (2023). Programmable Tissue Folding Patterns in Structured Hydrogels. Adv. Mater.2300017 https://doi.org/10.1002/adma.202300017.

28. Shi, N., Li, Y., Chang, L., Zhao, G., Jin, G., Lyu, Y., Genin, G.M., Ma, Y., and Xu, F. (2021). A 3D, Magnetically Actuated, Aligned Collagen Fiber Hydrogel Platform Recapitulates Physical Microenvironment of Myoblasts for Enhancing Myogenesis. Small Methods *5*, 2100276. https://doi.org/10.1002/smtd.202100276.

29. Yadid, M., Hagel, M., Labro, M.B., Le Roi, B., Flaxer, C., Flaxer, E., Barnea, A.R., Tejman-Yarden, S., Silberman, E., Li, X., et al. (2023). A Platform for Assessing Cellular Contractile Function Based on Magnetic Manipulation of Magnetoresponsive Hydrogel Films. Adv. Sci.2207498 https://doi.org/10.1002/advs.202207498.

30. Asgeirsson, D.O., Christiansen, M.G., Valentin, T., Somm, L., Mirkhani, N., Nami, A.H., Hosseini, V., and Schuerle, S. (2021). 3D magnetically controlled spatiotemporal probing and actuation of collagen networks from a single cell perspective. Lab Chip *21*, 3850–3862. https://doi.org/10.1039/D1LC00657F.

31. Uslu, F.E., Davidson, C.D., Mailand, E., Bouklas, N., Baker, B.M., and Sakar, M.S. (2021). Engineered Extracellular Matrices with Integrated Wireless Microactuators to Study Mechanobiology. Adv. Mater. *33*, 2102641. https://doi.org/10.1002/adma.202102641.

32. Frontera, W.R., and Ochala, J. (2015). Skeletal Muscle: A Brief Review of Structure and Function. Calcif. Tissue Int. *96*, 183–195. https://doi.org/10.1007/s00223-014-9915-y.

33. Sambasivan, R., and Tajbakhsh, S. (2015). Adult skeletal muscle stem cells. Vertebrate Myogenesis *56*, 191–213. https://doi.org/10.1007/978-3-662-44608-9.

34. Raman, R. (2019). Modeling muscle. Science *363*, 1051.

35. Raman, R. (2021). Engineered neuromuscular actuators for medicine, meat, and machines. MRS Bull. *46*, 522–533. https://doi.org/10.1557/s43577-021-00122-3.

36. Ricotti, L., Trimmer, B., Feinberg, A.W., Raman, R., Parker, K.K., Bashir, R., Sitti, M., Martel, S., Dario, P., and Menciassi, A. (2017). Biohybrid actuators for robotics : A review of devices actuated by living cells. Sci. Robot. *2*, eaaq0495. https://doi.org/10.1126/scirobotics.aaq0495.

37. Iberite, F., Gruppioni, E., and Ricotti, L. (2022). Skeletal muscle differentiation of human iPSCs meets bioengineering strategies: perspectives and challenges. NPJ Regen. Med. *7*, 23. https://doi.org/10.1038/s41536-022-00216-9.

38. Lloyd, P., Onaizah, O., Pittiglio, G., Vithanage, D.K., Chandler, J.H., and Valdastri, P. (2022). Magnetic Soft Continuum Robots With Braided Reinforcement. IEEE Rob. Autom. Lett. *7*, 9770–9777. https://doi.org/10.1109/LRA.2022.3191552.

39. Kim, Y., Yuk, H., Zhao, R., Chester, S.A., and Zhao, X. (2018). Printing ferromagnetic domains for untethered fast-transforming soft materials. Nature *558*, 274–279. https://doi.org/10.1038/s41586-018-0185-0.

40. Nagamine, K., Kawashima, T., Ishibashi, T., Kaji, H., Kanzaki, M., and Nishizawa, M. (2010). Micropatterning contractile C2C12 myotubes embedded in a fibrin gel. Biotechnol. Bioeng. *105*, 1161–1167. https://doi.org/10.1002/bit.22636.

41. Kloxin, A.M., Kloxin, C.J., Bowman, C.N., and Anseth, K.S. (2010). Mechanical properties of cellularly responsive hydrogels and their experimental determination. Adv. Mater. *22*, 3484–3494. https://doi.org/10.1002/adma.200904179.

42. Raman, R., Cvetkovic, C., Uzel, S.G.M., Platt, R.J., Sengupta, P., and Kamm, R.D. (2016). Optogenetic skeletal muscle-powered adaptive biological machines. Proc. Natl. Acad. Sci. USA *113*, 3497–3502. https://doi.org/10.1073/pnas.1516139113.

43. Raman, R., Grant, L., Seo, Y., Cvetkovic, C., Gapinske, M., Palasz, A., Dabbous, H., Kong, H., Pinera, P.P., and Bashir, R. (2017). Damage, Healing, and Remodeling in Optogenetic Skeletal Muscle Bioactuators. Adv. Healthcare Mater. *6*, 1700030. https://doi.org/10.1002/adhm.201700030.

44. Cvetkovic, C., Raman, R., Chan, V., Williams, B.J., Tolish, M., Bajaj, P., Sakar, M.S., Asada, H.H., Saif, M.T.A., and Bashir, R. (2014). Three-dimensionally printed biological machines powered by skeletal muscle. Proc. Natl. Acad. Sci. USA *111*, 10125–10130. https://doi.org/10.1073/pnas.1401577111.

45. Raman, R., Cvetkovic, C., and Bashir, R. (2017). A modular approach to the design, fabrication, and characterization of muscle-powered biological machines. Nat. Protoc. *12*, 519–533. https://doi.org/10.1038/nprot.2016.185.

46. Altomare, L., Gadegaard, N., Visai, L., Tanzi, M.C., and Farè, S. (2010). Biodegradable microgrooved polymeric surfaces obtained by photolithography for skeletal muscle cell orientation and myotube development. Acta Biomater. *6*, 1948–1957. https://doi.org/10.1016/j.actbio.2009.12.040.

47. Bauer, A., Gu, L., Kwee, B., Li, W.A., Dellacherie, M., Celiz, A.D., and Mooney, D.J. (2017). Hydrogel substrate stress-relaxation regulates the spreading and proliferation of mouse myoblasts. Acta Biomater. *62*, 82–90. https://doi.org/10.1016/j.actbio.2017.08.041.

48. Grant, L., Raman, R., Cvetkovic, C., Ferrall-Fairbanks, M.C., Pagan-Diaz, G.J., Hadley, P., Ko, E., Platt, M.O., and Bashir, R. (2018). Long-term cryopreservation and revival of tissue engineered skeletal muscle. Tissue Eng. *25*, 1023–1036. https://doi.org/10.1089/ten.TEA.2018.0202.

49. Eugenis, I., Wu, D., and Rando, T.A. (2021). Cells, scaffolds, and bioactive factors: Engineering strategies for improving regeneration following volumetric muscle loss. Biomaterials *278*, 121173. https://doi.org/10.1016/j.biomaterials.2021.121173.

50. Osaki, T., Uzel, S.G.M., and Kamm, R.D. (2020). On-chip 3D neuromuscular model for drug screening and precision medicine in neuromuscular disease. Nat. Protoc. *15*, 421–449. https://doi.org/10.1038/s41596-019-0248-1.

51. Bajaj, P., Reddy, B., Millet, L., Wei, C., Zorlutuna, P., Bao, G., and Bashir, R. (2011). Patterning the differentiation of C2C12 skeletal myoblasts. Integr. Biol. *3*, 897–909. https://doi.org/10.1039/c1ib00058f.

52. Armstrong, J.P.K., Puetzer, J.L., Serio, A., Guex, A.G., Kapnisi, M., Breant, A., Zong, Y., Assal, V., Skaalure, S.C., King, O., et al. (2018). Engineering Anisotropic Muscle Tissue using Acoustic Cell Patterning. Adv. Mater. *30*, e1802649. https://doi.org/10.1002/adma.201802649.

53. Ko, E., Yu, S.J., Pagan-Diaz, G.J., Mahmassani, Z., Boppart, M.D., Im, S.G., Bashir, R., and Kong, H. (2019). Matrix Topography Regulates Synaptic Transmission at the Neuromuscular Junction. Adv. Sci. *6*, 1801521. https://doi.org/10.1002/advs.201801521.

54. Mohammadzadeh, S., and Lejeune, E. (2023). SarcGraph: A Python package for analyzing thecontractile behavior of pluripotent stem cell-derived-cardiomyocytes. JOSS *8*, 5322. https://doi.org/10.21105/joss.05322.

55. Lam, M.T., Huang, Y.C., Birla, R.K., and Takayama, S. (2009). Microfeature guided skeletal muscle tissue engineering for highly organized 3-dimensional free-standing constructs. Biomaterials *30*, 1150–1155. https://doi.org/10.1016/j.biomaterials.2008.11.014.

56. Bian, W., and Bursac, N. (2009). Engineered skeletal muscle tissue networks with controllable architecture. Biomaterials *30*, 1401–1412. https://doi.org/10.1016/j.biomaterials.2008.11.015.

57. Zhao, R., Boudou, T., Wang, W.-G., Chen, C.S., and Reich, D.H. (2013). Decoupling Cell and Matrix Mechanics in Engineered Microtissues Using Magnetically Actuated Microcantilevers. Adv. Mater. *25*, 1699–1705. https://doi.org/10.1002/adma.201203585.

58. Rousseau, E., Raman, R., Tamir, T., Bu, A., Srinivasan, S., Lynch, N., Langer, R., White, F.M., and Cima, M.J. (2023). Actuated tissue engineered muscle grafts restore functional mobility after volumetric muscle loss. Biomaterials *302*, 122317. https://doi.org/10.1016/j.biomaterials.2023.122317.

59. Chandorkar, Y., Bastard, C., Di Russo, J., Haraszti, T., and De Laporte, L. (2022). Cells feel the beat – temporal effect of cyclic mechanical actuation on muscle cells. Appl. Mater. Today *27*, 101492. https://doi.org/10.1016/j.apmt.2022.101492.

60. Sakar, M.S., Neal, D., Boudou, T., Borochin, M.A., Li, Y., Weiss, R., Kamm, R.D., Chen, C.S., and Asada, H.H. (2012). Formation and optogenetic control of engineered 3D skeletal muscle bioactuators. Lab Chip *12*, 4976–4985. https://doi.org/10.1039/c2lc40338b.

61. Sunadome, K., Erickson, A.G., Kah, D., Fabry, B., Adori, C., Kameneva, P., Faure, L., Kanatani, S., Kaucka, M., Dehnisch Ellström, I., et al. (2023). Directionality of developing skeletal muscles is set by mechanical forces. Nat. Commun. *14*, 3060. https://doi.org/10.1038/s41467-023-38647-7.

62. Das, S.L., Sutherland, B.P., Lejeune, E., Eyckmans, J., and Chen, C.S. (2022). Mechanical response of cardiac microtissues to acute localized injury. Am. J. Physiol. Heart Circ. Physiol. *323*, H738–H748. https://doi.org/10.1152/ajpheart.00305.2022.

63. Bradski, G.R., and Kaehler, A. (2011). Learning OpenCV: Computer Vision with the OpenCV Library 1. ed., [Nachdr.] (O'Reilly).

64. Bouguet, J.-Y. (2001). Pyramidal Implementation of the A ne Lucas Kanade Feature Tracker Description of the Algorithm (Intel Corporation).

65. Shi, J.; Tomasi (1994). Good features to track. In 1994 Proceedings of IEEE Conference on Computer Vision and Pattern Recognition, pp. 593–600. https://doi.org/10.1109/CVPR.1994.323794.

DEVICE, Volume *1*

Supplemental information

Mechanically programming anisotropy in engineered muscle with actuating extracellular matrices

Brandon Rios, Angel Bu, Tara Sheehan, Hiba Kobeissi, Sonika Kohli, Karina Shah, Emma Lejeune, and Ritu Raman

Supplementary Information

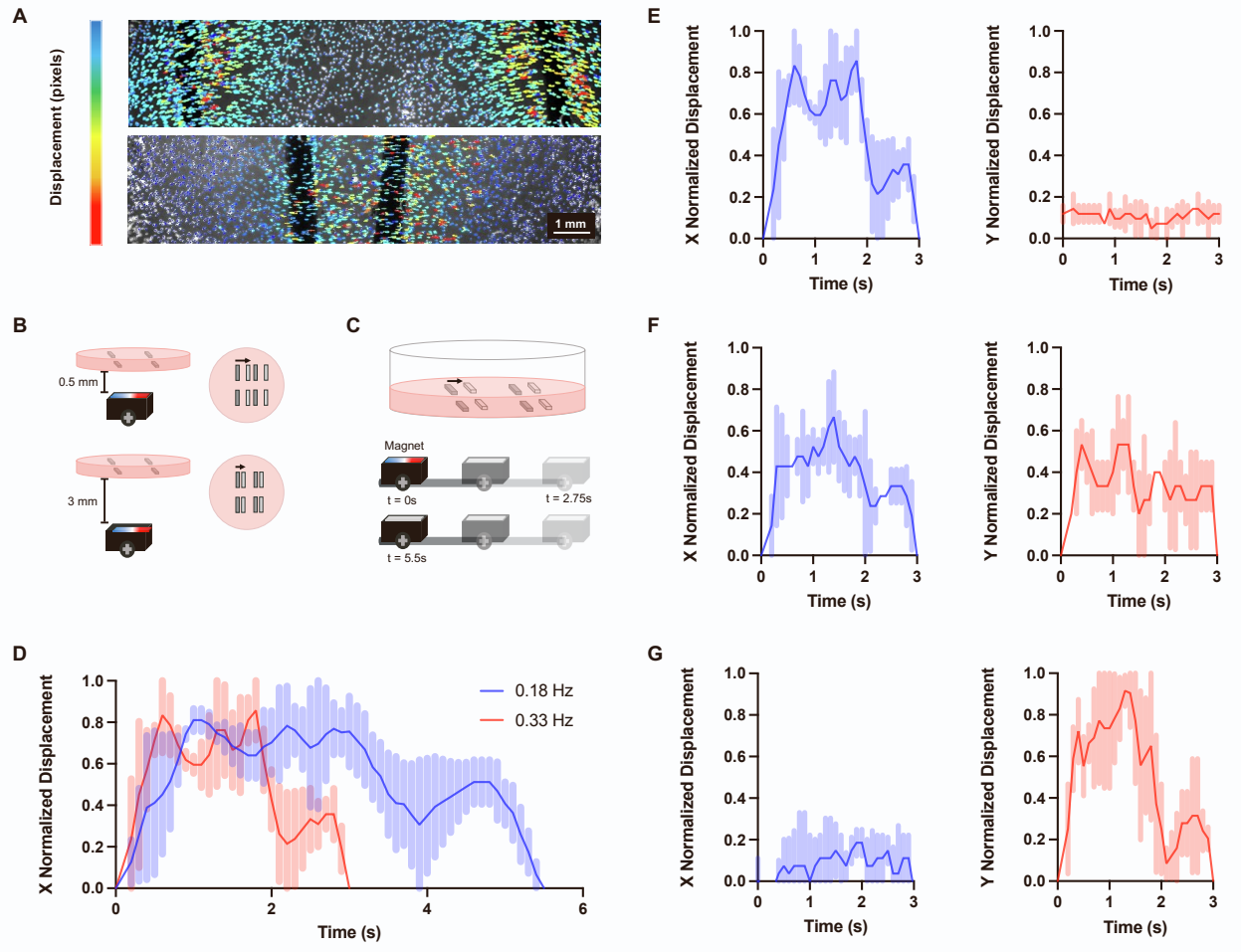

Supplemental Figure 1. Optimization of MagMA parameters. A) Optimization of magnetic microparticle placement within hydrogels shows more uniform deformation gradients are obtained when microparticles are spaced 2mm apart in the x-direction, as compared to larger spacings. **B)** Schematic showing impact of increasing distance between magnet and hydrogel. **C)** Schematic showing impact of reducing magnet actuation speed. **D)** Experimental data showing impact of reducing magnet actuation speed from 0.33 Hz to 0.18 Hz. **E)** Normalized x and y displacement of gel in response to magnet actuation along the x-axis, 0°. **F)** Normalized x and y displacement of gel in response to magnet actuation at 45°. **G)** Normalized x and y displacement of gel in response to magnet actuation along the y-axis, 90°.